Proceedings of ASME Turbo Expo 2011
GT2011
June 6-10, 2011, Vancouver, British Columbia, Canada

GT2011-46281

COMPARISON BETWEEN A CFD CODE AND A THREE-CONTROL-VOLUME MODEL FOR LABYRINTH SEAL FLUTTER PREDICTIONS

R. Phibel
Vibration UTC
Imperial College
London SW7 2BX, UK

L. di Mare
Vibration UTC
Imperial College
London SW7 2BX, UK

ABSTRACT

Labyrinth seals are extensively used in turbomachinery to control flow leakage in secondary air systems. While a large number a studies have been performed to investigate the leakage and rotordynamics characteristics of these seals, the studies on their aeroelastic stability remain scarce. Little is known about this phenomenon and the design methods are limited to a stability criterion which does not take into account many of the parameters which are known to influence labyrinth seal aeroelastic stability. As a consequence the criterion can be unreliable or overly pessimistic. The alternative to this criterion is the use of CFD methods which, although reliable, are computationally expensive. This paper presents a three-control-volume (3CV) bulk-flow model specifically developed for flutter calculations in labyrinth seals. The model is applied to a turbine labyrinth seal of a large diameter aero-engine and the results are compared to those of a CFD analysis. Conclusions are drawn on the potential of this 3CV model for design purposes.

NOMENCLATURE

b	fin tip thickness
c	clearance
E	total energy
F	inviscid fluxes
f/f_{ac}	mechanical-to-acoustic frequency ratio
H	total enthalpy
h	height of interfin cavity $h = h_2 + h_3$
h_2	height of CV2 (sum of steady-state part and perturbation)
h_3	height of CV3 (sum of steady-state part and perturbation)
L	cavity length
p'	pressure fluctuation
p_{ref}	reference pressure
Q	vector of conservative variables
R_c	radius of curvature
w_{aero}	aerodynamic work
x/p	nondimensional axial location of pivot point

Greek symbols

γ	angle of pitching motion
Π	inlet/outlet pressure ratio
ρ	density

Subscripts

A	CV1 inlet
B	CV1 outlet/CV2 inlet
C	CV2 outlet
R	rotor surface
SL	dividing streamline

1 Introduction

In rotating machinery, unavoidable clearances exist between rotating and stationary components. These clearances must be sealed to control flow leakage, which represents a loss to the working cycle, to prevent hot gas ingestion in turbine cavities as mentioned by Ludwig [1] (rim sealing), and avert contamination of the engine with oil from the bearing compartments

(Whitlock [2]). Aero engines still rely heavily on labyrinth seals for this purpose.

Fluid-structure interactions in these seals can lead to instabilities such as rotor whirl (Childs [3]), or seal flutter. The mechanism of seal flutter is as follows: the vibration of one seal member (rotor or stator) in its natural mode induces a change in seal clearance which can excite the flow in the inter-fin or upstream/downstream cavities. If the phase is adequate, the flow perturbations feed energy back into the motion and the vibrations are amplified. Alford [4, 5] determined that the support side of the seal had a critical influence on stability. Lewis et al. [6], who studied experimentally and analytically the stability of a turbofan engine labyrinth seal, showed that the seal clearance was another critical parameter. Abbott [7] found that seal aerolastic stability depended also on the ratio of the seal natural frequency to the acoustic frequency of the inter-fin cavities.

Most of the analysis tools presented in the literature to investigate seal flutter were based on bulk-flow models The first attempt to use a bulk-flow model for seal flutter predictions was presented by Ehrich [8]. He used a single-cavity single-control-volume bulk-flow model to derive a stability parameter. The outlet tooth was assumed choked which limited the validity of the model to high pressure ratios. When applying his model to actual seal designs, he observed a number of discrepancies which he attributed to the omission of the circumferential flow in his analysis. Prokop'ev and Nazarenko [9] studied the self-excited vibration of a plane labyrinth seal model as Ehrich. They did not suppose the outlet fin choked, thus extending the validity of the analysis to lower pressure ratios. They investigated the influence of the volume of the chambers, the pressure drop across the seal, the clearance, the seal rigidity and the location of the support. However, their model suffered from the same flaw as Ehrich's model since it did not consider the tangential flow, making the validity of the results questionable for turbomachinery seals. The single-control-volume model used by Lewis et al. [6] included the circumferential flow in the analysis. He reported good correlations between the predictions of his analytical model and the behaviour observed in engine test. Abbott [7] used a bulk-flow model similar to the model of Lewis. He successfully used this model to derive the frequency ratio stability criterion still in use today. Srinivasan et al. [10] extended the work of Lewis et al. [6] and Abbott [7] to take into account the flexibility of both seal members. They solved the complex eigenvalue problem of the coupled fluid-structure system made by the seal stator, the seal rotor and the leakage flow in-between to obtain the system modes and the logarithmic decrement. Using this model, they showed that when there was a match between rotor and stator frequency, there was a sudden change in logarithmic decrement toward a less stable system. Unfortunately, no comparison of the results of their model with experimental data or with the results of other models were presented.

All these models used a single control volume to represent the flow in an inter-fin cavity coupled with a leakage equation for the flow at the fin tips. In the field of rotor whirl, improved predictions of rotordynamic coefficients have been reported when using two- or three-control-volume models (Scharrer [11], Nordmann [12]). But none of these models has been applied to seal flutter predictions.

The purpose of this paper is to describe a three-control-volume bulk-flow model which has been developed for seal flutter predictions. The model uses a novel approach to define the two control volumes in the interfin cavity. Moreover comparisons are presented between predictions of the bulk-flow model and predictions from Computational Fluid Dynamics (CFD) methods.The CFD code used is AU3D developed at Imperial College. AU3D solves the unsteady Reynolds-averaged Navier-Stokes equations on unstructured grids. The Boussinesq approximation is used to compute the Reynolds stress tensor. In the present study, the eddy viscosity was given by the one-equation model of Spalart and Allmaras [13]. Temporal accuracy is ensured by using a dual time stepping technique. For flutter simulations, the mesh is moved at each time step to follow a prescribed motion of the structure. The resulting unsteady pressure is used to computed the aerodynamic work over a cycle of vibration. The simulations are stopped when a converged value of this aerodynamic work is obtained. More details on the CFD methods employed in this work can be found in another paper by the present authors [14].

In the following, we will present the bulk-flow model before showing some comparisons on two test cases: a single-cavity non rotating labyrinth seal and a four-fin rotating labyrinth seal representative of an engine design. The geometry for the latter case is shown in Fig. 1. The single-cavity case is obtained by isolating a cavity from the four-fin case.

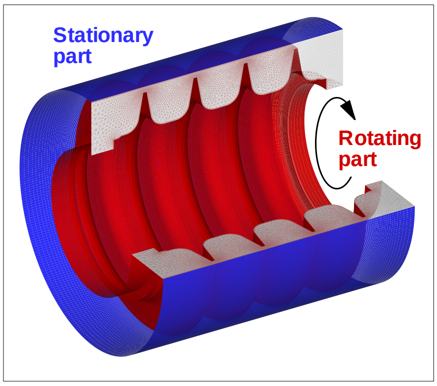

Figure 1. Labyrinth seal geometry

2 Bulk-flow model

2.1 Structural model

In the present study, we assume that the stator is fixed while the rotor is vibrating. In the labyrinth area of seals, the mode shape can be approximated by a rotation about a pivot point P as shown in Fig. 2. The angle γ' denotes the angle of the pitching

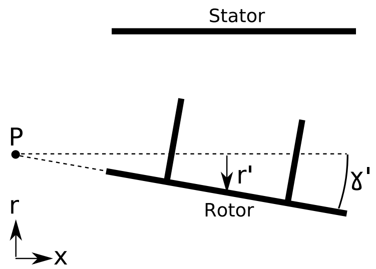

(a) View in (x,r) plane

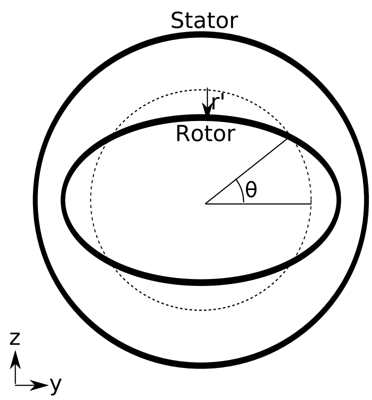

(b) View in (y,z) plane

Figure 2. Mode shape (here two-nodal-diameter mode).

motion. To model a travelling wave mode of angular frequency ω and nodal diameter number n, this angle is written (in complex form):

$$\gamma' = \gamma_0 e^{i(\omega t - n\theta)} \tag{1}$$

Since the model is linear the magnitude γ_0 is of no consequence and can be chosen arbitrarily. γ' will determine the radial motion of the rotor at each axial location $r'(x)$:

$$r'(x) = \gamma' (x - x_p) \tag{2}$$

where x_p is the axial location of the pivot point P. $r'(x)$ determines the change in clearance at the fin tips c' and the change in height of the interfin cavities h', which are used in the flow model presented in the following sections. At location x, $h'(x) = -r'(x)$ since the stator is fixed. x_p, ω and n are parameters in the model which can be varied to represent different mode shapes. The axial location of the pivot point x_p is varied to simulated different support locations. ω is varied to simulate different mechanical-to-acoustic frequency ratios. These two parameters are known to have a critical influence on seal aeroelastic stability. In the present study, n is kept constant and equal to 2.

2.2 Control volumes

The flow in a labyrinth seal is characterised by a jet flow emerging from the fin tips which drives a large recirculation in the interfin cavities (Fig. 4). Because of the seal rotation, which entrains the flow in the circumferential direction, this recirculation takes the form of an helicoidal vortex as described by Moore [15]. In this model, the flow in a labyrinth seal is described using three control volumes (Fig. 3):

(i) the fin tip area (CV1);
(ii) the through-flow area (CV2);
(iii) the cavity vortex area (CV3).

The last two control volumes are separated by the dividing streamline originating from the leading edge of the entrance fin (see Fig. 4). The advantage of this approach is that there is no mass flow between CV2 and CV3, which simplifies the governing equations. Moreover this division represents more closely the physical mechanism which is linked to an exchange of energy between the cavity area and the through-flow area. The difficulty lies in the modelling of the dividing streamline motion.

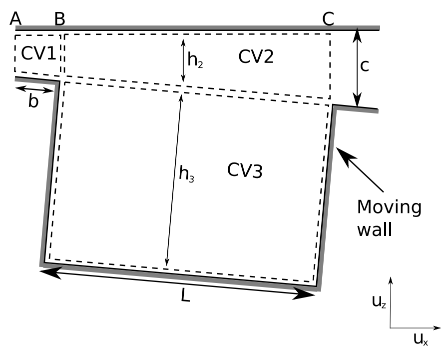

Figure 3. Control volumes.

2.3 Governing equations

The equations will be written for a two-dimensional flow in the (x,z) plane. There is no fundamental difference when writing them for an axisymmetric flow. u, v and w are the components of

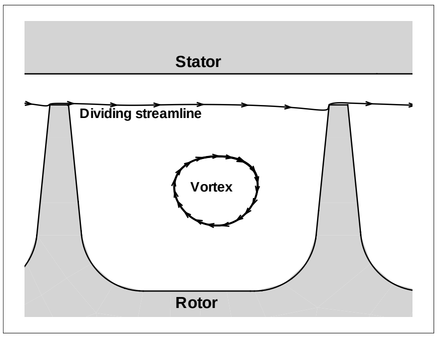

Figure 4. Steady-state flow pattern showing the dividing streamline.

velocity in the x, y and z direction respectively. A coordinate system is shown in Fig. 5. For the first and second control volumes,

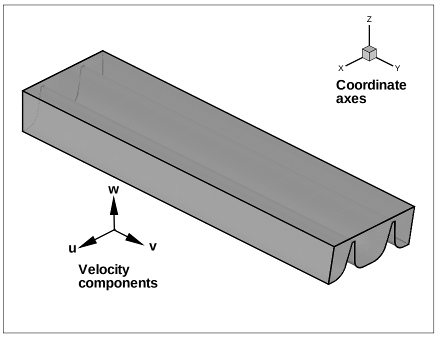

Figure 5. Coordinate system and corresponding velocity components.

we write the conservation of mass, axial momentum, tangential momentum and total energy. In the third control volume, there is no mean axial flow, and only the conservation of mass, tangential momentum and total energy are written. The viscous contributions are neglected in the present model. Some notations used in the following are shown in Fig. 3.

2.3.1 Control volume 1

The conservation of mass, momentum and energy in CV1 can be written in vector form:

$$\frac{\partial(Qc)}{\partial t}+\frac{\partial(Qvc)}{\partial y}+c\frac{\partial F_y}{\partial y}+F_{Ey}\frac{\partial c}{\partial y} = \frac{1}{b}\left[c_A F_A - c_B F_B + (c_B - c_A)F_{Rx})\right] + F_{Rz} \tag{3}$$

with:

$$Q=\begin{bmatrix}\rho\\ \rho u\\ \rho v\\ \rho E\end{bmatrix}, F_y=\begin{bmatrix}0\\0\\p\\pv\end{bmatrix}, F_{Ey}=\begin{bmatrix}0\\0\\0\\pv\end{bmatrix}, F_A=\begin{bmatrix}\rho_A u_A\\ \rho_A u_A^2+p_A\\ \rho_A u_A v_A\\ \rho_A u_A H_A\end{bmatrix},$$

$$F_B=\begin{bmatrix}\rho_B u_B\\ \rho_B u_B^2+p_B\\ \rho_B u_B v_B\\ \rho_B u_B H_B\end{bmatrix}, F_{Rx}=\begin{bmatrix}0\\p_R\\0\\0\end{bmatrix}, F_{Rz}=\begin{bmatrix}0\\0\\0\\p_R w_R\end{bmatrix}$$

2.3.2 Control volume 2

The equations for CV2 are similar to those of CV1, the clearance c being replace by the height h_2 of CV2, and the tip thickness b by the cavity length L:

$$\frac{\partial(Qh_2)}{\partial t}+\frac{\partial(Qvh_2)}{\partial y}+h_2\frac{\partial F_y}{\partial y}+F_{Ey}\frac{\partial h_2}{\partial y} = \frac{1}{L}\left[c_B F_B - c_C F_C + (c_C - c_B)F_{SLx}\right] + F_{SLz} \tag{4}$$

with:

$$F_C=\begin{bmatrix}\rho_C u_C\\ \rho_C u_C^2+p_C\\ \rho_C u_C v_C\\ \rho_C u_C H_C\end{bmatrix}, F_{SLx}=\begin{bmatrix}0\\p_{SL}\\0\\0\end{bmatrix}, F_{SLz}=\begin{bmatrix}0\\0\\0\\p_{SL}w_{SL}\end{bmatrix}$$

2.3.3 Control volume 3

In CV3, there is no (mean) axial flow and only the conservation of mass, tangential momentum and energy are written:

$$\frac{\partial(Qh_3)}{\partial t}+\frac{\partial(Qvh_3)}{\partial y}+h_3\frac{\partial F_y}{\partial y}+F_{Ey}\frac{\partial h_3}{\partial y} = F_R - F_{SL} \tag{5}$$

with:

$$Q=\begin{bmatrix}\rho\\ \rho v\\ \rho E\end{bmatrix}, F_y=\begin{bmatrix}0\\p\\pv\end{bmatrix}, F_{Ey}=\begin{bmatrix}0\\0\\pv\end{bmatrix},$$

$$F_R=\begin{bmatrix}0\\0\\p_R w_R\end{bmatrix}, F_{SL}=\begin{bmatrix}0\\0\\p_{SL}w_{SL}\end{bmatrix}$$

2.3.4 Interfaces between control volumes

The fluxes at interfaces A, B and C between CV1 and CV2 are obtained using Roe approximate Riemann solver (Hirsch [16]). Between CV2 and CV3, there is only a flux of energy F_{SL} via the radial motion of the dividing streamline. The pressure p_{SL} appearing is this flux is taken equal to the arithmetic average between the pressure in CV2 and the pressure in CV3. The velocity w_{SL} is provided by the model for the motion of the dividing streamline presented in Sect. 2.5.

2.4 Perturbation analysis

Assuming small motion of the rotor, the flow in the labyrinth can be written as the sum of the steady-state flow and a perturbation:

$$Q = \bar{Q} + Q' \tag{6}$$

with:

$$\bar{Q} = \begin{bmatrix} \bar{\rho} \\ \bar{\rho}\bar{u} \\ \bar{\rho}\bar{v} \\ \bar{\rho}\bar{E} \end{bmatrix}, Q' = \begin{bmatrix} \rho' \\ \bar{\rho}u' + \rho'\bar{u} \\ \bar{\rho}v' + \rho'\bar{v} \\ \bar{\rho}E' + \rho'\bar{E} \end{bmatrix}, \tag{7}$$

At first order, we obtain the following equations for the perturbed flow:

CV1:

$$\bar{Q}\frac{Dc'}{Dt} + \bar{c}\frac{DQ'}{Dt} + \bar{Q}\bar{c}\frac{\partial v'}{\partial y} + \bar{c}\frac{\partial F'_y}{\partial y} + \bar{F}_{Ey}\frac{\partial c'}{\partial y} = \frac{1}{b}\left[\bar{c}\left(F'_A - F'_B\right) + c'_A\bar{F}_A - c'_B\bar{F}_B + \left(c'_B - c'_A\right)\bar{F}_{Rx}\right] + F'_{Rz} \tag{8}$$

CV2:

$$\bar{Q}\frac{Dh'_2}{Dt} + \bar{h}_2\frac{DQ'}{Dt} + \bar{Q}\bar{h}_2\frac{\partial v'}{\partial y} + \bar{h}_2\frac{\partial F'_y}{\partial y} + \bar{F}_{Ey}\frac{\partial h'_2}{\partial y} = \frac{1}{L}\left[\bar{c}\left(F'_B - F'_C\right) + c'_B\bar{F}_B - c'_C\bar{F}_C + \left(c'_C - c'_B\right)\bar{F}_{SLx}\right] + F'_{SLz} \tag{9}$$

CV3:

$$\bar{Q}\frac{Dh'_3}{Dt} + \bar{h}_3\frac{DQ'}{Dt} + \bar{Q}\bar{h}_3\frac{\partial v'}{\partial y} + \bar{h}_3\frac{\partial F'_y}{\partial y} + \bar{F}_{Ey}\frac{\partial h'_3}{\partial y} = F'_R - F'_{SL} + F'_{ESC} \tag{10}$$

where:

$$\frac{D}{Dt} = \frac{\partial}{\partial t} + \bar{v}\frac{\partial}{\partial y} \tag{11}$$

F'_{ESC} represents an unsteady flux (of mass, momentum and energy) out of CV3 during vibrations when the dividing streamline loses contact with the outlet fin as illustrated in Fig. 6. In the model, this flux is written as a fraction of the steady-state flux at the outlet fin F_c and is proportional to the size of the unsteady gap between the dividing streamline and the outlet fin tip. Thus, we have:

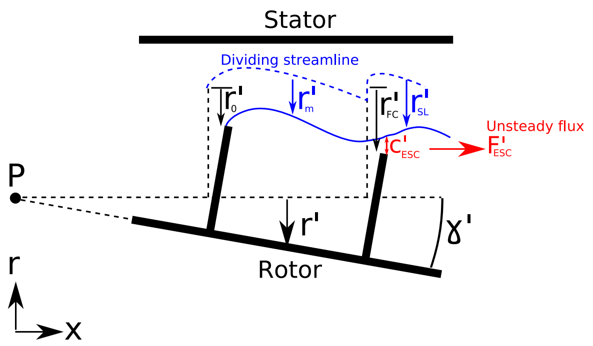

Figure 6. Unsteady flux out of CV3. During vibration the dividing streamline loses contact with the outlet fin causing a flux of mass, momentum and energy out of CV3 through the gap c'_{ESC}.

$$\frac{F'_{ESC}}{F_C} = \alpha\frac{c'_{ESC}}{\bar{c}} \tag{12}$$

where c'_{ESC} is the size of the unsteady gap. α is a constant of the model. The unsteady gap between the dividing streamline and the exit fin tip is modelled as follows:

$$c'_{ESC} = r'_{SL} - r'_{FC} \tag{13}$$

where r'_{SL} is the motion of the dividing streamline above the exit fin and r'_{FC} is the motion of the exit fin. The motion of the dividing streamline above the exit fin is influenced not only by the motion of the dividing streamline in the interfin cavity but also by the motion of the exit fin. To represent this in the model, r'_{SL} is written as a linear combination of the average motion of the dividing streamline in the cavity r'_m and the motion of the exit fin

r'_{FC}.

$$r'_{SL} = \lambda_1 r'_m + \lambda_2 r'_{FC} \tag{14}$$

λ_1 and λ_2 are weights representing the relative influence of the motion of the dividing streamline in the cavity and the motion of the exit fin on the motion of the dividing streamline above the exit fin.

The perturbed fluxes F'_A, F'_B and F'_C are obtained by performing a linearisation of the flux formula given by the Roe approximate Riemann solver.

The variation of the clearance at the fin tips c' is known from the mode shape. h'_2 and h'_3 are part of the unknowns. They are linked by the following relation:

$$h'_2 + h'_3 = h' \tag{15}$$

where h' is the variation of the cavity height which is known from the mode shape. An additional relation is required to complete the solution. It is provided by the equation governing the motion of the dividing streamline.

2.5 Equation governing the motion of the dividing streamline

An approximate equation for the motion of the dividing streamline can be obtained by writing the momentum balance along the dividing streamline in streamline coordinates and carrying a perturbation analysis. The momentum balance in the direction normal to the streamline for an inviscid fluid reads:

$$\frac{\partial p}{\partial n} = \rho \frac{v_m^2}{R_c} \tag{16}$$

where $\frac{\partial p}{\partial n}$ is the normal pressure gradient, ρ is the density, v_m the magnitude of the velocity and R_c the radius of curvature. This indicates that the streamline curvature, and thus its location, is influenced by the value of the normal pressure gradient, the magnitude of the velocity and the value of the density along the dividing streamline. Starting from this equation and carrying a perturbation analysis yields a linear relationship of the form:

$$\frac{r'_m}{c} = \alpha_r \frac{r'_0}{c} + \alpha_\rho \frac{\rho'}{\bar{\rho_2}} + \alpha_v \frac{(v^2)'}{\bar{u_2}^2} + \alpha_p \frac{\frac{\partial p'}{\partial n}}{\bar{\rho_2}\bar{u_2}^2/R_c} \tag{17}$$

where r'_m is the average radial motion of the dividing streamline, r'_0 is the motion of the entrance fin leading edge, ρ' and $(v^2)'$ are the fluctuations in density and velocity (squared) on the dividing streamline, $\frac{\partial p'}{\partial n}$ is the fluctuation in normal pressure gradient on the streamline. $\bar{\rho_2}$, $\bar{u_2}$ are the average velocity and density in CV2. The equation is written in non-dimensional form to obtain coefficients of order unity. We need to evaluate the fluctuations along the streamline from the values of the fluctuations in the through-flow and cavity vortex control volumes. It seems reasonable to write the fluctuations in density and velocity along the dividing streamline as weighted averages of the fluctuations in the through-flow control volume and in the cavity vortex control volume:

$$\rho' = \beta_{2\rho}\rho'_2 + \beta_{3\rho}\rho'_3 \tag{18}$$
$$(v^2)' = \beta_{2v}(v_2^2)' + \beta_{3v}(v_3^2)' \tag{19}$$

where the coefficients α and β are weights. The obvious choice for the normal pressure gradient would be to write:

$$\frac{\partial p'}{\partial n} = \frac{p'_2 - p'_3}{\delta} \tag{20}$$

where δ is some characteristic length for the pressure gradient (similar to a shear layer thickness). However poor results are obtained with the latter choice. This might be because δ should not be constant. Better agreement is obtained by writing:

$$\frac{\partial p'}{\partial n} = \frac{\beta_{2p}p'_2 - \beta_{3p}p'_3}{\delta} \tag{21}$$

The values of the constants α, β and δ are adjusted with the aid of CFD results. This leads to the following complex equation for the perturbation of CV2 height $h'_2 = -r'_m$ (using the fact that $r'_0 = -c'_A$):

$$\begin{aligned} h'_2 &+ \frac{\alpha_r \bar{c}}{\bar{\rho_2}}\left(\beta_{2\rho}\rho'_2 + \beta_{3\rho}\rho'_3\right) + 2\frac{\alpha_v \bar{c}}{\bar{u_2}}\beta_{2v}u'_2 \\ &+ \frac{\alpha_p \bar{c}}{\bar{\rho_2}\bar{u_2}^2\delta/R_c}\left(\beta_{2p}p'_2 - \beta_{3p}p'_3\right) = \alpha_r c'_A \end{aligned} \tag{22}$$

This equation completes the system given by Eq.(8) to (10) which can now be solved.

2.6 Solution procedure

We look for a travelling wave solution of the form $Q' = Q_0 e^{i(\omega t - ky)}$, where k is the wave number. The partial derivatives in Eq.(8) to (10) can then be replaced by:

$$\frac{\partial}{\partial t} = i\omega \tag{23}$$

$$\frac{\partial}{\partial y} = -ik \tag{24}$$

This results in a system of complex algebraic linear equations which can be inverted directly since the system is small. For the boundary conditions, we assume that the flow at the inlet and outlet remains unperturbed. These boundary conditions are imposed using a linearised form of Riemann invariants.

3 Results

In this section, results obtained with the analytical model are compared to CFD results. The test cases considered are a single-cavity labyrinth seal and a four-fin labyrinth seal. For both cases, the vibration mode is a 2ND forward travelling mode. The mode shape is a rotation about a pivot point which is moved from upstream to downstream to model seals supported on their high- and low-pressure side. The location of the pivot point is identified by its axial coordinate divided by the pitch x/p; $x/p = 0$ when the pivot point is in the middle of the seal. The mechanical-to-acoustic frequency ratio f/f_{ac}, which is a critical parameter for seal flutter, is varied by modifying the frequency of the mode. The comparisons are made in terms of the aerodynamic work w_{aero} (nondimensionalised by a reference value w_{ref}). To this end, the amplitude of motion is set to 1% of the clearance in the model as in CFD simulations. The steady-state value in the control volumes of the analytical model are obtained by averaging CFD steady-state results over the relevant areas.

3.1 Single-cavity labyrinth

Results concerning the influence of the pivot point location at three frequency ratios are presented in Fig. 7. There is a reasonably good agreement between the 3 CV model and CFD results at the two lower frequency ratios. At a frequency ratio of 1.5, the 3 CV model tends to overestimate the aerodynamic work.

Fig. 8 shows results on the influence of the frequency ratio when the pivot point in on the high-pressure side (HPS) and low-pressure side (LPS). The tendency of the 3 CV model to overestimate the aerodynamic work at high frequency ratio is clearly visible. The analytical model is able to predict the correct stability but the magnitude of the aerodynamic work is overestimated. Fig. 9 and 10 compare the magnitude and phase of the unsteady pressure predicted by the 3 CV model and computed with CFD as a function of the frequency ratio for a LPS mode. There are some important discrepancies in the magnitude. These discrepancies become more severe as the frequency ratio is increased.

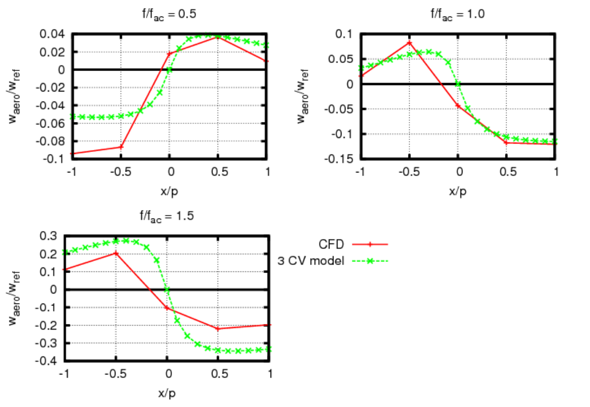

Figure 7. Influence of pivot point location on aerodynamic work - Single-cavity labyrinth seal.

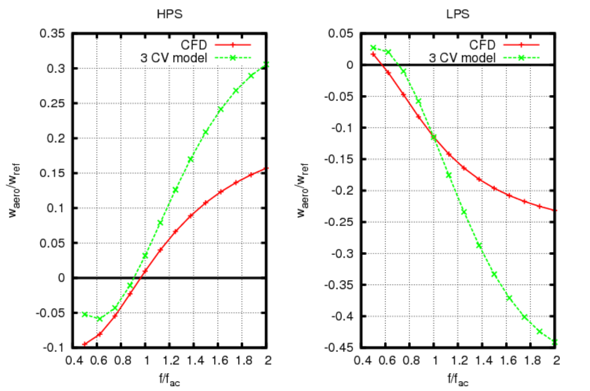

Figure 8. Influence of frequency ratio on aerodynamic work - Single-cavity labyrinth seal.

This explains the discrepancies on the aerodynamic work at high frequency ratios. The first cavity has a singular behaviour because of the importance of the vena contracta at the entrance fin. In the analytical model, all fin tips are treated in the same manner. This could account for the discrepancies observed on this single-cavity case.

Results on the influence of the pressure ratio are presented in Fig. 11 For most cases, the predictions of the analytical model agree qualitatively with CFD results. The model is able to predict the change of stability at low pressure ratio for the HPS mode at $f/f_{ac} = 1$. At $f/f_{ac} = 1.5$, the curve of aerodynamic work given by the analytical model is similar in shape but shifted towards positive values of the work; consequently the analytical model predicts a change of stability at a lower pressure ratio. For the LPS mode at $f/f_{ac} = 0.5$, the analytical model does not predict the change of sign of the work at the lowest pressure ra-

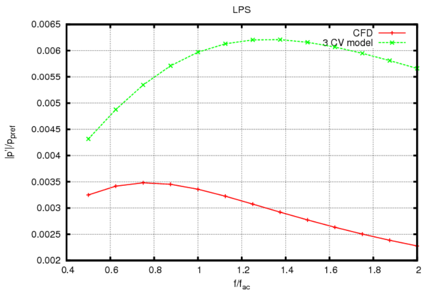

Figure 9. Influence of frequency ratio on unsteady pressure magnitude - Single-cavity labyrinth seal - LPS.

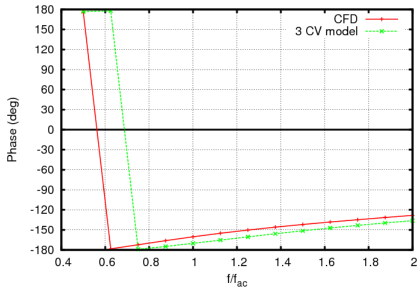

Figure 10. Influence of frequency ratio on unsteady pressure phase - Single-cavity labyrinth seal - LPS.

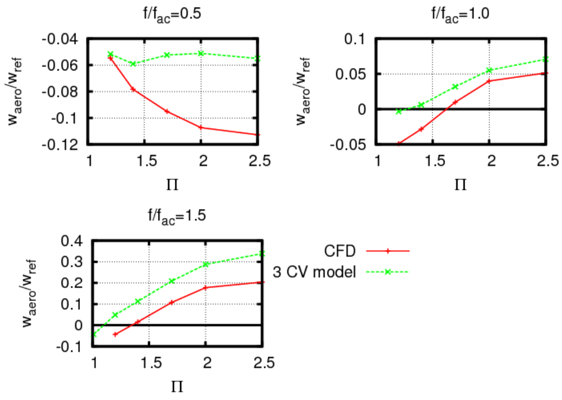

(a) HPS mode

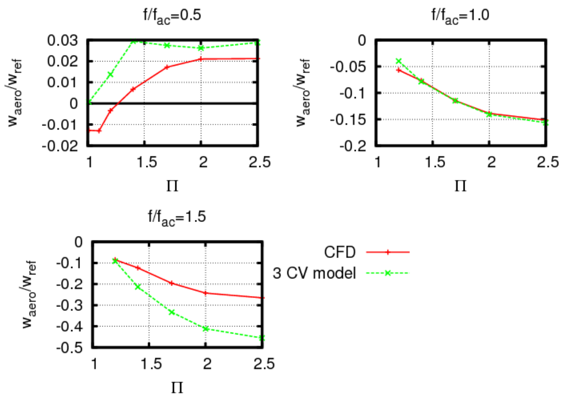

(b) LPS mode

Figure 11. Influence of pressure ratio on aerodynamic work - Single-cavity labyrinth seal.

tio; instead the aerodynamic work tends to zero. This discrepancy can be caused either by an error on the magnitude or on the phase of the unsteady pressure. The magnitude and phase of the unsteady pressure computed by CFD and the analytical model for this mode are presented in Fig. 12. The magnitude of the unsteady pressure is in good agreement between the model and CFD. The phase is well predicted by the analytical model at the pressure ratios above 1.4. Below this pressure ratio, CFD simulations predict a sharp increase of the phase which crosses the phase -180 degree and thus the stability changes. This sharp increase is not reproduced by the analytical model.

There are some important discrepancies at the lowest frequency ratio for the HPS mode. The magnitude and phase of the unsteady pressure computed by CFD and the analytical model for this mode are presented in Fig. 13. The magnitude of the unsteady pressure is overestimated by the model at low pressure ratio and the model fails to reproduce the sharp decrease in phase; this is similar to the behaviour observed for the LPS mode discussed above. At high pressure ratio, the magnitude is reasonably well predicted by the analytical. However there are 4 degrees of difference on the phase. This difference is enough to cause the observed discrepancies on the aerodynamic work.

3.2 Four-fin labyrinth

Plots of the aerodynamic work as a function of the pivot point location and the frequency ratio are produced for the 4-fin labyrinth seal in Fig. 14 and Fig. 15. Here the compliance with CFD results is good.

Fig. 16 compares the phase distribution in the labyrinth predicted by CFD and obtained with the three-control-volumes models for three locations of the pivot point. The results of a two-control-volume model previously developed by the present authors are also included. This model did not include a control volume for the fin tip. The frequency ratio is equal to one as for Fig. 14. The three-control-volumes model is able to reproduce the significant change of phase between adjacent cavities contrary to the two-control-volume model; this results in phase predictions closer to CFD.

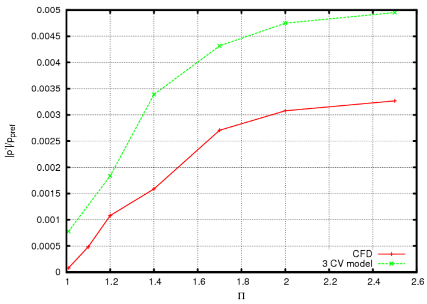

(a) Magnitude

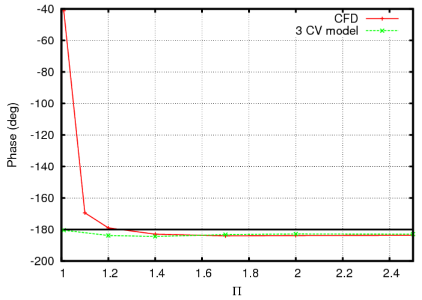

(b) Phase

Figure 12. Influence of pressure ratio on unsteady pressure magnitude and phase - Single-cavity labyrinth seal - LPS mode - $f/f_{ac} = 0.5$.

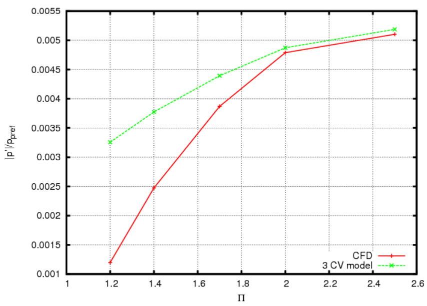

(a) Magnitude

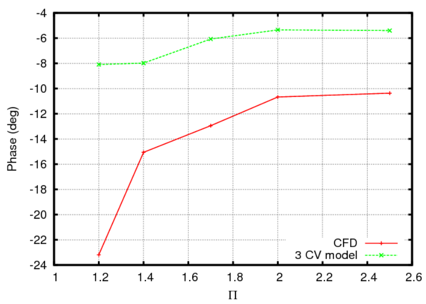

(b) Phase

Figure 13. Influence of pressure ratio on unsteady pressure magnitude and phase - Single-cavity labyrinth seal - HPS mode - $f/f_{ac} = 0.5$.

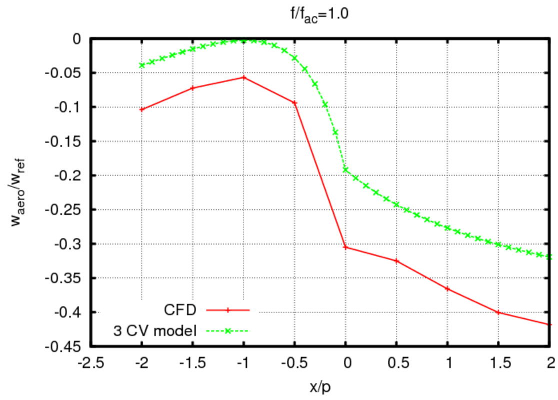

Figure 14. Influence of pivot point location on aerodynamic work - Four-fin labyrinth seal.

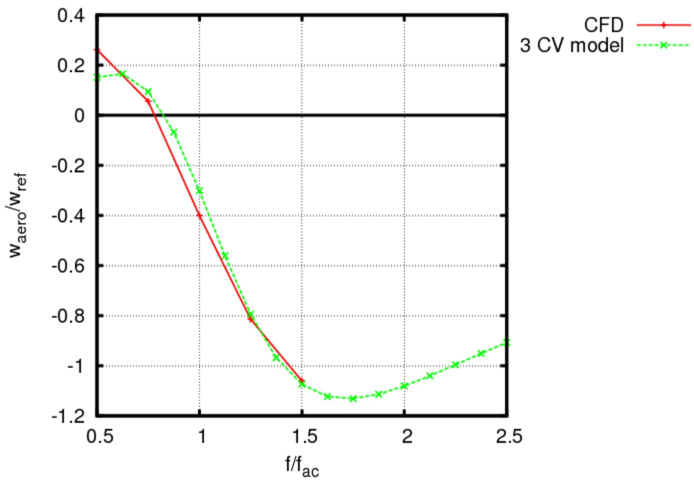

Figure 15. Influence of frequency ratio on aerodynamic work - Four-fin labyrinth seal.

4 Conclusions

A three-control-volume analytical model for labyrinth seal flutter has been presented. On a single-cavity labyrinth seal case, the model gives reasonably good results at mechanical-to-acoustic frequency ratios lower than one but tends to over-estimate the aerodynamic work at higher frequency ratios. A possible cause could be the lack of modelling of the vena contracta at the first fin tip. The results on a 4-fin labyrinth seal case are in good agreement with CFD results. In particular, the three-control-volume model is able to reproduce the significant change of phase between adjacent cavities contrary to a two-control-volume model previously developed by the present authors. The model could be used to carry out quick paramet-

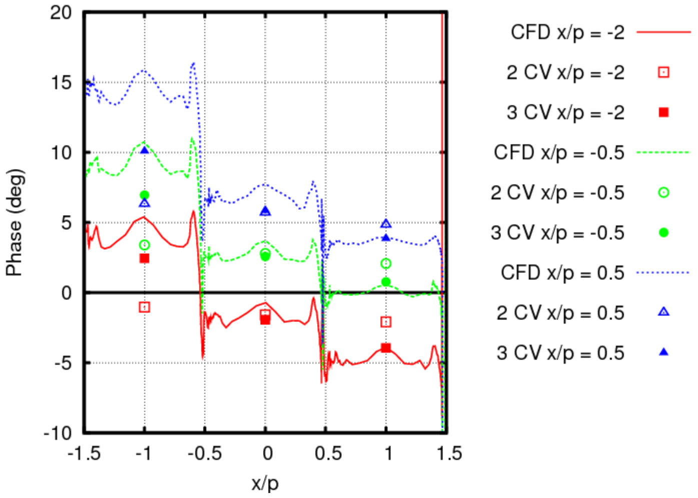

Figure 16. Phase distribution in the labyrinth for three pivot locations at a frequency ratio of 1 - Four-fin labyrinth seal.

ric studies. For quantitative predictions, improvements are still needed if the model is to replace completely CFD simulations.

5 Acknowledgements

The authors acknowledge Rolls-Royce plc and EPSRC for funding this research.

REFERENCES

[1] Ludwig, L., 1978. "Gas Path Sealing in Turbine Engines". In AGARD-CP-237.

[2] Whitlock, D., 1978. "Oil Sealing of Aero Engine Bearing Compartments". In AGARD-CP-237.

[3] Childs, D., 1993. *Turbomachinery Rotordynamics, Phenomena, Modeling, and Analysis*. John Wiley & Sons, Inc.

[4] Alford, J., 1964. "Protection of Labyrinth Seals From Flexural Vibration". *Journal of Engineering for Power*, **86**, pp. 141–147.

[5] Alford, J., 1967. "Protecting Turbomachinery from Unstable and Oscillatory Flows". *Journal of Engineering for Power*, **89**, pp. 513–528.

[6] Lewis, D., Platt, C., and Smith, E., 1979. "Aeroelastic Instability in F100 Labyrinth Air Seals". *Journal of Aircraft*, **16**(7), pp. 484–490. also AIAA Paper 78–1087.

[7] Abbott, D. R., 1980. "Advances in Labyrinth Seal Aeroelastic Instability Prediction and Prevention". ASME Paper 80-GT-151.

[8] Ehrich, F., 1968. "Aeroelastic Instability in Labyrinth Seals". *Journal of Engineering for Power*, October, pp. 369–374.

[9] Prokop'ev, V. I., and Nazarenko, G. M., 1973. "Aeroelastic Vibrations in Labyrinth Seals". *Strength of Materials*, **5**, pp. 798–802.

[10] Srinivasan, A., Arnoldi, R., and Dennis, A., 1984. "Aeroelastic Instabilities in Labyrinth Air Seal Systems". ASME Paper 84-GT-169.

[11] Scharrer, J. K., 1987. "A comparison of experimental and theoretical results for labyrinth gas seals". PhD thesis, Texas A&M University.

[12] Nordmann, R., and Weiser, P., 1990. "Evaluation of Rotordynamic Coefficients of Look-Through Labyrinths By Means of a Three Volume Bulk Flow Model". In Proceedings of Rotordynamic Instability Problems in High Performance Turbomachinery, pp. 147–163. NASA CP-3122.

[13] Spalart, P. R., and Allmaras, S. R., 1994. "A One-Equation Turbulence Model for Aerodynamic Flows". *La Recherche Aerospatiale*(1), pp. 5–21.

[14] Phibel, R., di Mare, L., Green, J., and Imregun, M., 2009. "Numerical Investigation of Labyrinth Seal Aeroelastic Stability". In Proceedings of ASME Turbo Expo 2009. GT2009-60017.

[15] Moore, J., 2003. "Three-Dimensional CFD Rotordynamics Analysis of Gas Labyrinth Seals". *Journal of Vibration and Acoustics*, **125**, October, pp. 427–433.

[16] Hirsch, C., 1990. *Numerical Computation of Internal and External Flows, Volume 2, Computational Methods for Inviscid and Viscous Flows*. Wiley.